

Electronic structure and stabilities of Ni-doped germanium nanoclusters: a density functional modeling study

Kapil Dhaka · Ravi Trivedi · Debashis Bandyopadhyay

Received: 19 June 2012 / Accepted: 12 November 2012 / Published online: 14 December 2012
© Springer-Verlag Berlin Heidelberg 2012

Abstract The present study reports the geometry, electronic structure, growth behavior and stability of neutral and ionized nickel encapsulated germanium clusters containing 1–20 germanium atoms within the framework of a linear combination of atomic orbital density functional theory (DFT) under a spin polarized generalized gradient approximation. In the growth pattern, Ni-capped Ge_n and Ni-encapsulated Ge_n clusters appear mostly as theoretical ground state at a particular size. To explain the relative stability of the ground state clusters, variation of different parameters, such as average binding energy per atom (BE), embedding energy (EE) and fragmentation energy (FE) of the clusters, were studied together with the size of the cluster. To explain the chemical stability of the clusters, different parameters, e.g., energy gap between the highest occupied and lowest unoccupied molecular orbitals (HOMO–LUMO gap), ionization energy (IP), electron affinity (EA), chemical potential (μ), chemical hardness (η), and polarizability etc. were calculated and are discussed. Finally, natural bond orbital (NBO) analysis was applied to understand the electron counting rule applied in the most stable Ge_{10}Ni cluster. The importance of the calculated results in the design of Ge-based superatoms is discussed.

Keywords Clusters and nanoclusters · Binding energy · Density functional theory · Electron affinity · Embedding energy · Ionization potential

Introduction

The study of the electronic structure and properties of nanoclusters is an extremely active area of research due to its importance in nanoscience and nanotechnology. In the past 10–12 years, a considerable amount of research has focused on semiconductor based nanomaterials [1–8]. Recently, small and medium size metal encapsulated semiconductor clusters have been investigated due to the potential interest of the physical and chemical processes taking place at the metal–semiconductor interface [9–13]. In general, pure semiconductor clusters are chemically reactive [14] and it is a challenging job to model and verify experimentally physically and chemically stable semiconductor nanoclusters. Among different possibilities, encapsulation of a transition metal (TM) in a pure semiconductor cage-like structure is currently the most popular and effective method. Such clusters enhance stability because the TM atom absorbs the dangling bonds present on the semiconductor cages [15, 16]. Simultaneously, the cluster exhibits a wide range of electronic properties by varying the doping elements. The first experimental contribution to this field was made by Beck [17, 18], who used a laser vaporization supersonic expansion technique and found that TMs such as Cr, Mo W, etc., in Si clusters enhanced the stability of the doped clusters. Hiura et al. [7] reported the formation of a series of Si cages with TM atoms Hf, Ta, W, Re, Ir, etc. Ohara et al. [19] used photoelectron spectroscopy and a chemical-probe method to study the geometric and electronic structures of negatively charged Tb doped Si_n clusters, and found that Tb atom always remains encapsulated inside the Si clusters of size $n=10$. Recently, Bandyopadhyay [20–28] reported an extensive study of the electronic structure, growth behavior, and different physical and chemical properties of pure and TM-doped semiconductor nanoclusters ($\text{TM}@M$, $\text{TM}=\text{Ti, Zr, Hf, Ni, Cu, Sc}$ and V , $M=\text{Si}$ or

K. Dhaka · R. Trivedi · D. Bandyopadhyay (✉)
Department of Physics, Birla Institute of Technology and Science,
Pilani, Rajasthan 333031, India
e-mail: debashis.bandy@gmail.com

Ge, $n=1$ to 20). It was found that the metal-doped semiconductor clusters show maximum stability in closed-shell electron configuration with 20-valence electrons in the clusters by taking into account the fact that each germanium or silicon atoms contributes one electron to the bonding. Koyasu et al. [29] studied the structural and electronic properties of metal silicon TM@Si_{16} (TM=Sc, Ti, and V) by mass spectrometry and anion photoelectron spectroscopy. Kawamura et al. [30] studied the growth behavior of the TM-doped silicon cluster, TM@Si_n (TM=Ti, Zr and Hf, $n=8$ –16). Their results suggest continuous aggregation until the size reached $n=16$ —the optimal cage for metal-encapsulated silicon clusters with those TM elements. It was found that neutral TiSi_{16} clusters had a closed-shell electron configuration with a large energy gap between the highest occupied and lowest unoccupied molecular orbitals (HOMO–LUMO gap). Recently, a detailed investigation on the thermochemistry and electronic affinity of Si_nLi ($n=1$ –10) clusters and their anions was reported by Yanh et al. [31]. Different global search methods, based on density functional theory (DFT) of metal-doped silicon clusters were reported by Marchal et al. [32] and Karamanis et al. [33]. Zhang et al. [34] investigated TM-doped semiconductor germanium clusters, TM@Ge_n ($n=14$ –16), and found that the growth behaviors of metal-encapsulated germanium clusters differ from those of metal-encapsulated silicon clusters. Wang and Hall [35] reported the growth behavior and chemical properties of nickel-doped germanium clusters of different sizes. Theoretical studies of pure and halogen-doped germanium clusters are also important in the field of semiconductor clusters [36–39]. Some recent studies on hydrogenated germanium clusters should also be mentioned because their behavior differs from that of pure and TM-doped germanium clusters [40]. The study of the size dependent variation of different parameters such as ionization potential, electron affinity etc. of hydrogenated TM-doped germanium nanoclusters has made important contributions to this field. Following developments in this field and the recent discovery of superatoms [41, 42], the present study made an effort to explain the enhanced stability of Ge_{10}Ni cluster in Ge_nNi ($n=1$ –20) series by studying different physical and chemical properties of the theoretical ground state clusters in each size using DFT. Small size range Ni-doped germanium clusters have been studied theoretically

before [35], but due to the smaller size range the latter study could not provide clear growth behavior, structural and electronic properties of the series. Therefore, a study of the range in the present study is important from a realistic point of view and would be helpful to compare with the experimentally obtained data over a wide size range in future. The main focus of the present study was to explain the thermodynamic stability of clusters in neutral and charged states along with their chemical properties in detail.

Computational methods

In the present theoretical work, all calculations were performed within the framework of linear combination of atomic orbitals DFT. The exchange-correlation potential contributions are incorporated into the calculation using the spin-polarized generalized gradient approximation (GGA) functional proposed by Lee, Yang and Parr popularly known as B3LYP [43]. Different basis sets were used for germanium and nickel with effective core potential using the Gaussian'03 [44] program package. The standard LanL2DZdp and LanL2DZ basis sets were used for germanium and nickel to express the molecular orbitals (MOs) of all atoms as linear combinations of atom-centered basis functions. LanL2DZdp (taken from EMSL basis set exchange library) is a double- ζ , 18-valence electron basis set with a LANL effective core potential (ECP) and with polarization function [45–47]. All geometry optimizations were performed with no symmetry constraints. During optimization, it is always possible that a cluster with a particular guess geometry can get trapped in a local minimum of the potential energy surface. To avoid this, several initial geometries in a particular size with different spin states (singlet to quintet) are taken as input in the calculation to search for the theoretical ground-state (GS) isomer during the optimization. In order to check the validity of the applied methodology, trial calculations are carried out on Ge–Ge, Ni–Ni and Ge–Ni dimers. The calculated Ge–Ge bond length in the germanium dimer at triplet spin state (ground state) is 2.44 Å (with a lowest frequency of 250 cm^{-1}). This is very close to the values obtained by several groups as shown in Table 1. The bond length and the lowest frequency of the Ge–Ni dimer in the triplet spin state (ground state) were

Table 1 Bond length and frequency of different dimers

Dimer	Bond length (Å)	Lowest frequency (cm^{-1})
Ge-Ge	2.36–2.42 [48–53], 2.46 [54], 2.57 [55], 2.44 ^a	258 [G. Frudakis, personal communication], 250 ^a
Ge-Ni	2.248 [56], 2.32 ^a	239 [57], 236 ^a
Ni-Ni	2.06 [58], 2.155[59], 2.13 [60], 2.20 [61], 2.36 [23], 235 ^a	210±25[59], 236 [23], 232 ^a

^a Present work

obtained in the present calculation as 2.32 Å and 236 cm⁻¹, respectively. The values reported by other groups are 2.25 Å and 239 cm⁻¹ as shown in Table 1. The bond length of the triplet ground state Ni–Ni dimer obtained in the present method is 2.35 Å, and the corresponding frequency is 232 cm⁻¹. These values are also close to the values reported in the literature (Table 1). Comparing the bond lengths and lowest frequencies of different dimers, the present method of calculation can be taken as being appropriate for nickel-doped germanium clusters. The optimized electronic structure is obtained by solving the Kohn-Sham equations self-consistently [62] using the default optimization criteria of the Gaussian'03 program [44]. The initial input geometries of the clusters used in the calculations were constructed on the basis of the reported optimized geometries [26–28] and also from their modified versions. With increasing size of clusters, the number of isomers in a particular size increases exponentially. So it is a challenging job to search for a ground-state cluster in a particular size. Tai and Nguyen [63] adopted a stochastic search method that covers a good number of isomeric structures and increases the chance of finding the ground state geometry. Several other very effective global search methods are also available, including a genetic algorithm to search for ground state geometries [64–66]. To check the stabilities of the structures, a frequency check calculation of the harmonic vibrations of the clusters is also done. If any imaginary frequency was found in a particular vibrational mode, relaxation was performed along that mode until a true local minimum was obtained. Geometry optimizations were carried out to a convergence limit of 10⁻⁷ Hartree in the total optimized energy. The optimized geometries as well as the electronic properties of the clusters in each size were obtained from the calculated program output.

Results and discussion

Our previous report [20] presented a detailed study of the growth behavior of pure germanium cluster. Here, we discuss the growth behavior of nickel-doped germanium clusters.

Growth of hybrid Ni@Ge_n nanoclusters

Theoretically calculated optimized isomers of Ni@Ge_n clusters within the size range $n=1-20$ are shown in Fig. 1a. In the present study, a number of isomers were calculated at each size. Only selected isomers with energy close to the supposed ground state structures are presented in Fig. 1a. It is well known that nickel is ferromagnetic material with an [Ar] 3d⁸4s² electronic configuration, whereas germanium has an [Ar]3d¹⁰4s²4p² electronic configuration. The germanium

cluster makes a sp³d² type of hybridization with the doped nickel atom in most cases. There is a strong mixing affinity between the sp-orbitals of germanium with the TM d-orbitals to form sp³d² hybridization. When the germanium atom in the stable cluster is replaced by a TM atom, or when the pure germanium cage is doped by a TM atom, the doped TM atom absorbs the dangling bonds present on the surface of the pure germanium cages. Recent studies [20–28] have shown that metal-doped cage-like isomers are important because of their relatively higher stability compared to pure semiconductor clusters and also due to the wide variation in electronic properties, which are useful for different applications. A bare nickel atom has a triplet spin multiplicity. Therefore, in the present calculations, all Ni@Ge_n guess structures were optimized at different spin states starting from singlet to quintet until there is a drop in optimized energies to check whether the spin moment of nickel inside the cage could survive under bonding with germanium or not. Wang and Han [35] found that the theoretical ground state of the Ge–Ni dimer with C_{∞v} point group symmetry can hold a triplet spin state. The immediate next higher size also show a triplet ground state. Four different isomers were optimized at this size with the triangular isomer in C_{2v} point group symmetry as ground state. The other two structures are linear chain structures in D_{2h} and C_{2v} point group symmetry as shown in Fig. 1a. Out of the four isomers in Ni@Ge₃, the isomer with the triplet bend rhombus in the ¹A₁ state with C_{2v} point group symmetry is the theoretical ground state. Other isomers are two different pyramidal structures with very close degenerate states. Seven stable isomers were found in Ge₄Ni. Of these, four low energy isomers are presented in Fig. 1a. The Ni-capped bent rhombus in the ¹A₁ electronic state with C_{2v} point group symmetry is found as the ground state. The other three structures are planar rhombus with a tail as shown in Fig. 1a. The first three low-energy Ge₅Ni isomers are shown in Fig. 1a out of a number of optimized structures in this size. The optimized ground state structure (5C in Fig. 1a) in C_s full point group symmetry can be obtained by replacing one capped germanium atom by Ni in the Ge₆ bi-capped pyramidal isomer. Three low-energy optimized isomers in the Ge₆Ni series are shown in Fig. 1a. These structures can be obtained by adding a Ni atom to Ge₆(A) or by replacing a Ni atom from Ge₇(A) as reported in our previous study [20]. Replacing one capped germanium atom with Ni from a bi-capped hexagonal Ge₈ cluster gives the boat-like optimized ground state shown as 7D in Fig. 1a. The first size that can absorb the nickel atom partially is Ge₈Ni (Fig. 1a). The ground state isomer is in the ¹A₁ electronic state, with C_{2v} point group symmetry and in singlet spin state. The first structure that can enclose the nickel atom endohedrally is Ni@Ge₉. Starting from $n=9$, all other isomers with $n>9$ absorb the nickel atom endohedrally and these structures always have lower optimized energies compared to the same sized exohedrally doped structures as calculated. Therefore, in

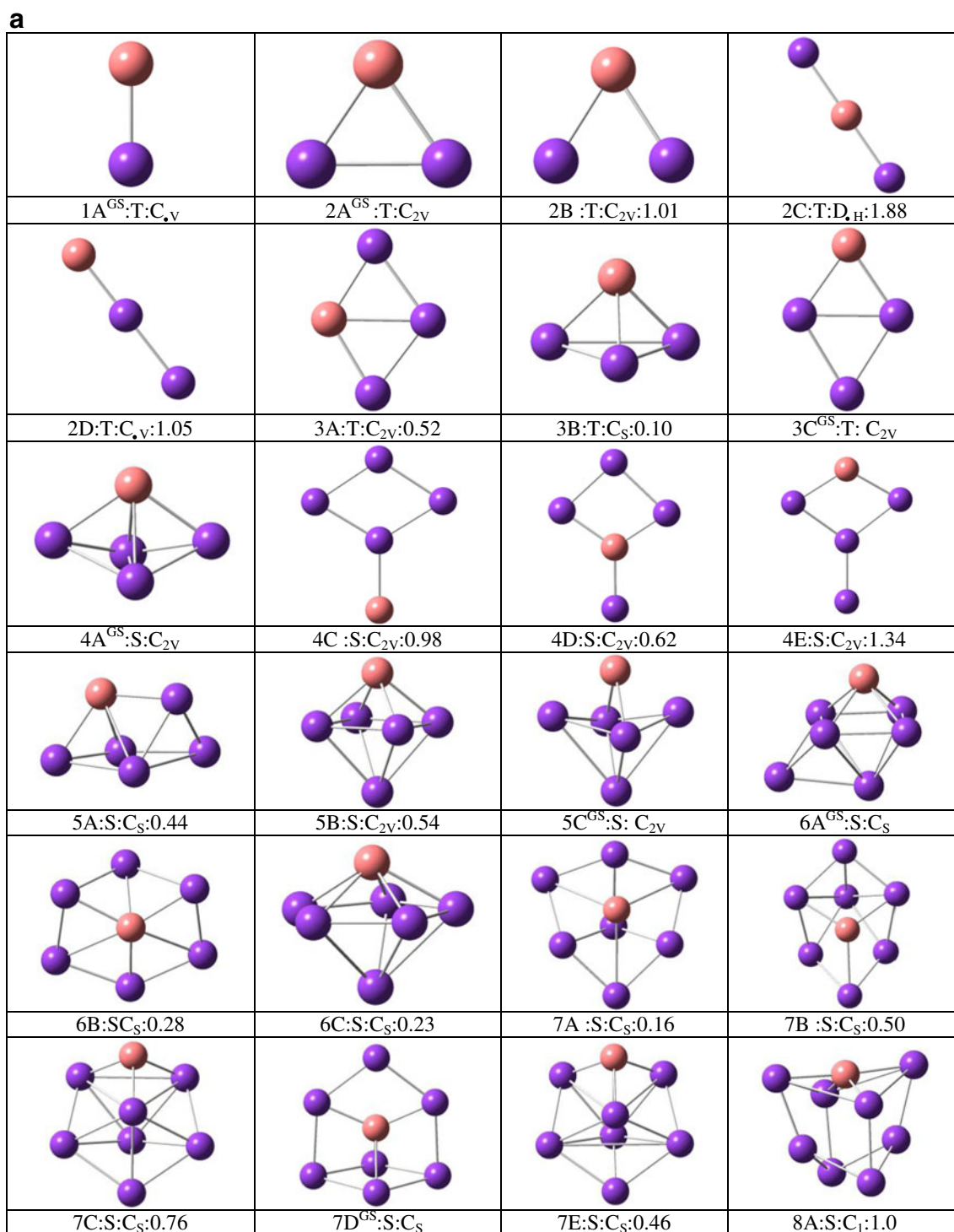


Fig. 1 **a** Optimized structures of neutral Ge_nNi ($n=1-20$) clusters with spin state (S singlet, T triplet), point group symmetry and energy with respect to the calculated ground state in each size. Purple balls

Germanium atoms, orange balls nickel atoms. **b** Different Valence orbitals of 20-electron ground state clusters

the present report, only endohedral-doped clusters are presented. The isomers labeled 9A, 9C and 9F in Fig. 1 are very similar with almost the same optimized energies. Several geometries are optimized in $n=10$ size to cover nearly all possible endohedral-doped structures. Of these, the

icosahedral structure (10A in Fig. 1a) in C_s point group symmetry is the supposed ground state. The endohedral Ni atom is almost at the center. The ten valence electrons of Ni make bonds with all ten germanium atoms in the cage. Because of the saturation of the dangling bonds this structure is

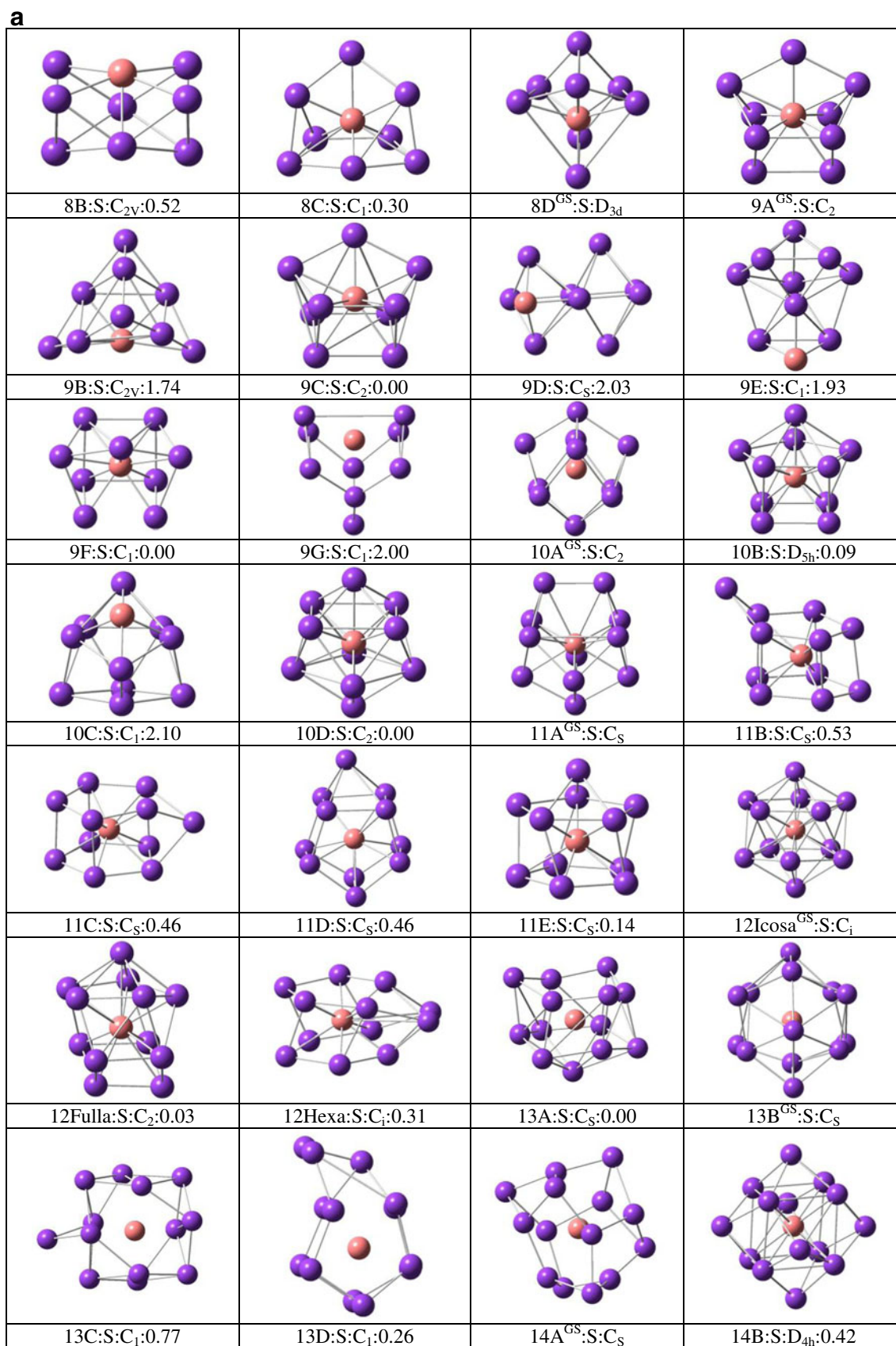


Fig. 1 (continued)

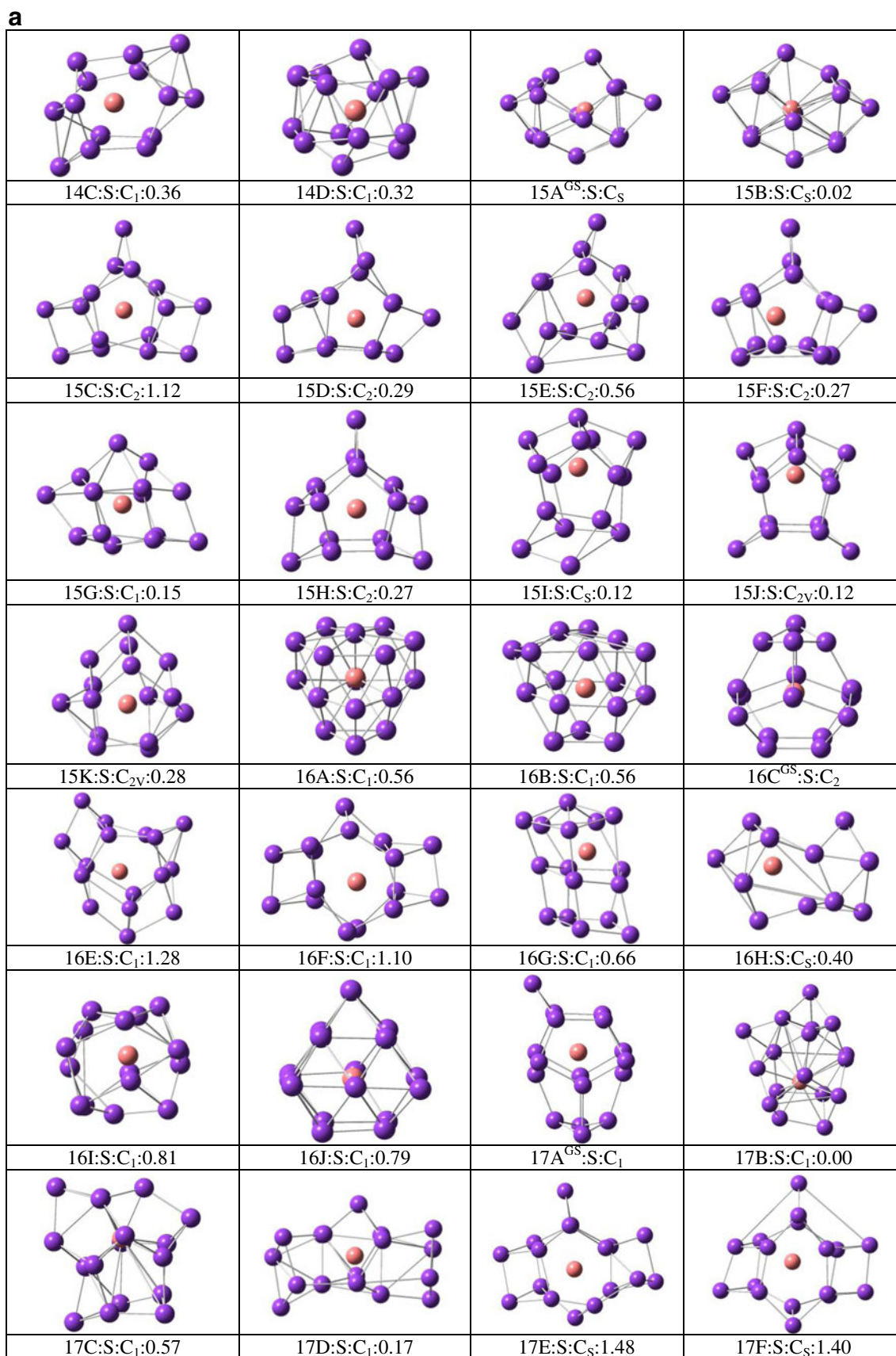


Fig. 1 (continued)

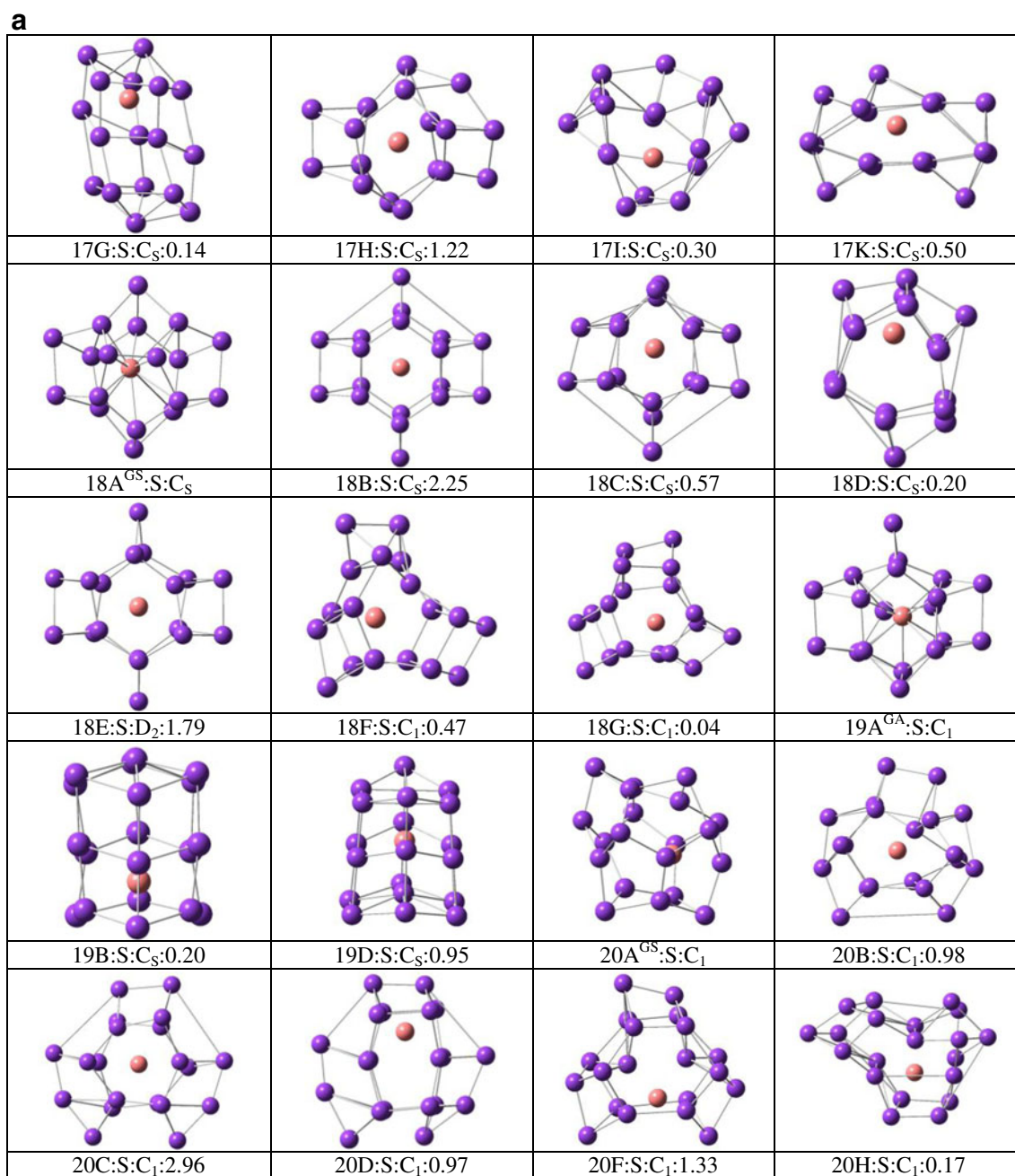
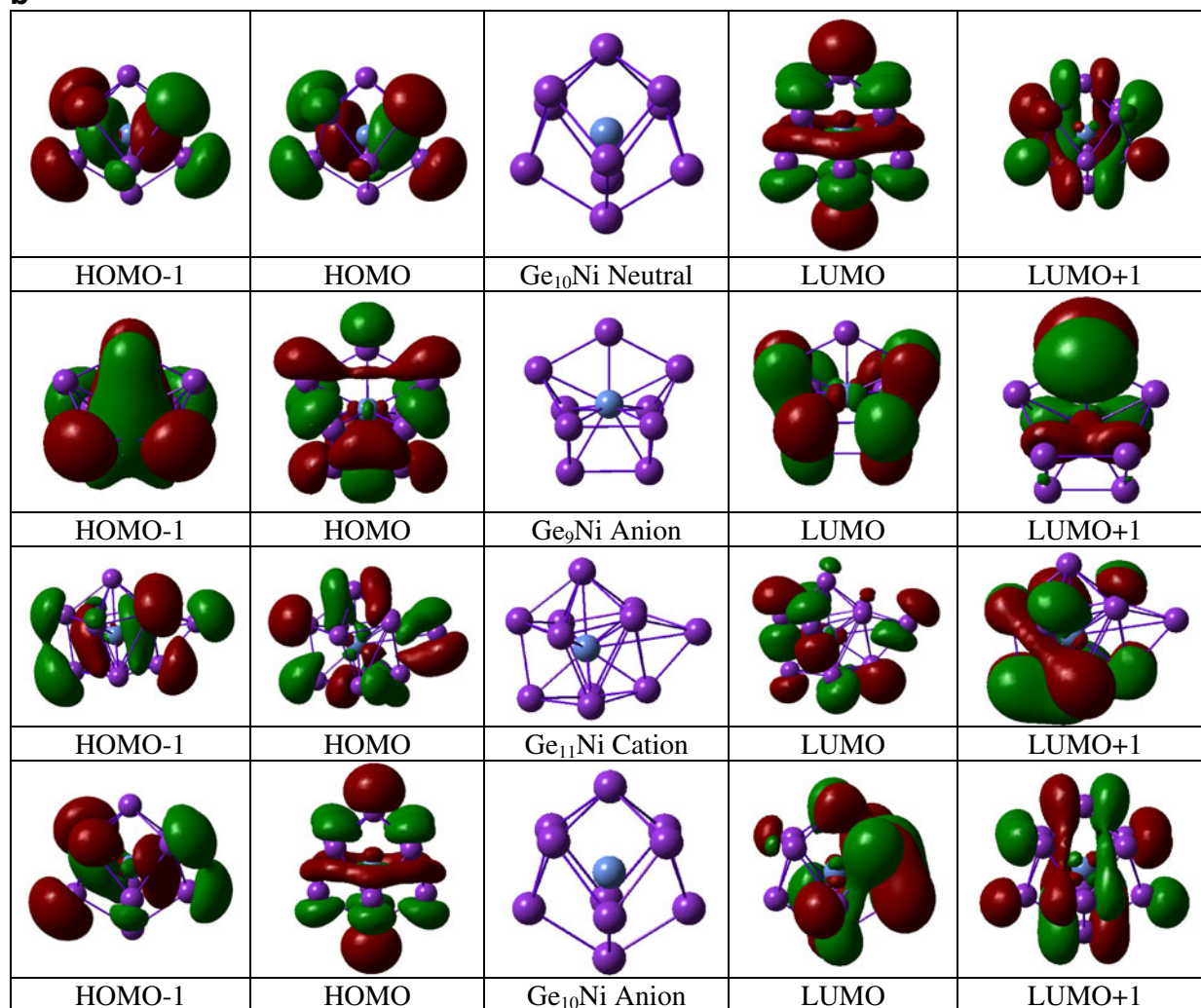


Fig. 1 (continued)

very stable and will be discussed further below. A slight modification of the ground state Ni@Ge₁₀ structure by adding a germanium atom gives the optimized ground state of Ni@Ge₁₁. The three calculated very common low-energy isomers of Ni@Ge₁₂ are hexagonal-prism-like, fullerene-like and icosahedral-like structures as shown in Fig. 1a. Both the ground state structures found with the size $n=10$ and 12 are icosahedral and usually very stable because of their symmetry, whereas the ground state structure for other values of n are relatively less symmetrical. This could explain the fluctuation of data in several parameters such as charge, chemical

potential, etc., with the increasing size of the clusters as presented below. The ground state we found in Ni@Ge₁₃ is a germanium-capped Ni@Ge₁₂ hexagonal prism structure. The structure looks like a bowl with a nickel atom inside. The calculated ground state Ni@Ge₁₄ has three-fold symmetry and is a combination of pentagons and rhombi. The other three structures are hexagonal prism-like structures. By adding a germanium atom to one of the vertices of the Ni@Ge₁₄ hexagonal pyramidal structure, the theoretical ground state of Ni@Ge₁₅ can be obtained. Other isomers in this size are small modifications of the pentagonal Ni@Ge₁₀ isomer with

b**Fig. 1** (continued)

additional five germanium atoms at different positions. Nine different optimized isomers are presented in Ni@Ge₁₆. The ground state in this size is a cage structure with C₂ symmetry, and is a combination of two widely separated squares and eight pentagons. Each square is connected to four pentagons separately. The isomer 16B in Fig. 1a can be constructed from a hexagonal Ge₁₂Ni prism isomer where one side is capped by a Ge₃ triangular plane and the other by a Ge atom. The total optimized energies of both of these isomers (16A and 16B) are very similar. Other isomers are not very symmetrical and their optimized energies are also much higher than the first three isomers in this series. A number of optimized isomers are calculated for Ge₁₇Ni. Among these optimized structures, ten isomers are presented in Fig. 1a. The guess geometry of the ground state isomer in $n=17$ can be obtained by adding one germanium atom with the one arm of the square in the ground state isomer 16C. The next three cage isomers 17B, 17C, and 17D can be obtained by optimizing the guessed structures

obtained by adding three Ge atoms to the ground-state isomer 14A at three different positions. The other structures in this size are modified 16F or 12Hexa geometries and are shown in Fig. 1a. The optimized isomers in Ge₁₈Ni can be explained with the help of 17E or 12Hexa isomers. The isomers 18A, 18B, 18C and 18E can be constructed from 17E by adding one Ge atom on the opposite side of the floating Ge atom and then by connecting it to the other Ge atoms in the cage. Adding four germanium atoms with the side arms of hexagonal Ge₁₂Ni structure yields the isomer 18D. Optimization after addition of three Ge–Ge dimers to three alternate side planes of the hexagonal Ge₁₂Ni geometry gives isomer 18G. Four different optimized isomers in Ge₁₉Ni are shown in Fig. 1a. The ground-state isomer 19A is obtained by adding one Ge atom to the ground-state isomer 18A. The isomers 19B and 19D are tube-like structures with hexagonal cross-section and a Ge capping. The ground-state isomer 20A of Ge₂₀Ni is a combination of 12 pentagons. Each side of a pentagon is

connected to another pentagon, so that every pentagon is linked to five other pentagons. The other two structures, 20B and 20C, can be obtained by adding two Ge atoms to the isomer 18E in different ways. 20D can be obtained by adding eight Ge atoms to the hexagonal Ge_{12}Ni structure, or by capping the closed side of the isomer 19B with an additional Ge atom. Other structures are very much distorted and their optimized energies are also much higher than the ground state isomer.

Upon examining the growth pattern of Ge_nNi clusters, it appears that cluster growth can be classified into three different categories. The first is Ni-capped structures, where the Ni atom is added to a small sized pure-Ge cluster to form Ge_nNi . In the second category, a Ge atom in the Ge_n cluster is replaced by a Ni to form Ge_{n-1}Ni cluster. Both categories are observed in the smaller cluster size range, where the cluster starts either from a Ge–Ge or from a Ge–Ni dimer; then a nickel or germanium atom is added directly to Ge_n or a Ge added to Ge_{n-1}Ni to form a Ge_nNi cluster. In the third category, the Ni atom is partially encapsulated in a Ge_nNi cluster. Complete encapsulation of the Ni atom by the Ge cluster is found in $n=9$ and above. After that, it is only possible to add a Ge atom to a Ge_{n-1}Ni cluster to form Ge_nNi . During this growth process, the shape of the cluster changes from two-dimensional to three-dimensional where the pure germanium cluster absorbs a nickel atom exohedrally or endohedrally. It was found that larger clusters prefer to retain the Ni atom as the encapsulated atom in Ge_nNi cages.

Electronic structures and stabilities of $\text{Ni}@\text{Ge}_n$ nanoclusters

The electronic structures and stabilities of $\text{Ni}@\text{Ge}_n$ nanoclusters are discussed here on the basis of variations in calculated physical and chemical parameters, i.e., binding energy (BE), HOMO–LUMO gap (or ΔE), embedding energy (EE), stability or the second-order difference in energy (Δ_2), ionization potential (IP), electron affinity (EA), and chemical potential

(μ) with cluster size (n). By monitoring the behavior of these parameters as the cluster size increases, we investigated whether or not electron counting can explain the relative stabilities of the clusters. To explore the relative stabilities of Ge_nNi clusters with increasing n , we first calculated various thermodynamic parameters of the clusters: BE, EE, ΔE , and Δ_2 .

Following our recent work [28], the average binding energy per atom of Ge_n or $\text{Ni}@\text{Ge}_n$ clusters is defined as: $\text{BE} = -(E_{\text{cluster}} - nE_{\text{Ge}} - E_{\text{Ni}})/(n+1)$, where BE is the average binding energy per atom of the cluster, and E_{Ge} , E_{Ni} and E_{cluster} are the energies of germanium and nickel and the ground state energy of the Ge_nNi cluster, respectively. For pure germanium clusters in the above equation, E_{Ni} is taken as zero and $n+1$ is replaced by n . The binding energies of charged clusters are also calculated using the same equation. The binding energies of different neutral and charged clusters, along with the binding energy of pure Ge clusters, are shown in Fig. 2. Both graphs show a rapid increase in the average binding energy per atom of the clusters in the small size range (for $n < 7$). This is because of the thermodynamic instability of smaller clusters. For clusters of size $n > 5$, the binding energy curve increases at a relatively slow rate with n , and finally saturate for the larger clusters ($n > 10$). For neutral clusters, the binding energy per atom in the saturation region ($n = 12\text{--}20$) varies within ± 0.1 eV, with the maximum binding energy occurring at $n = 10$, whereas the maximum binding energy is observed for anionic and cationic states at $n = 10$ and $n = 11$, respectively. According to the 18-electron counting rule, the binding energy and other physical parameters (discussed in the next section) should show a local maxima or minima at $n = 7, 8$ and 9 for anionic, neutral and cationic clusters, respectively, whereas according to the 20-electron counting rule, the binding energy and other physical parameters (discussed in the next section) should show a local maxima or minima at $n = 9, 10$ and 11 for anionic,

Fig. 2 Variation of binding energy of Ge_n and Ge_nNi clusters in neutral and different charged states with the cluster size

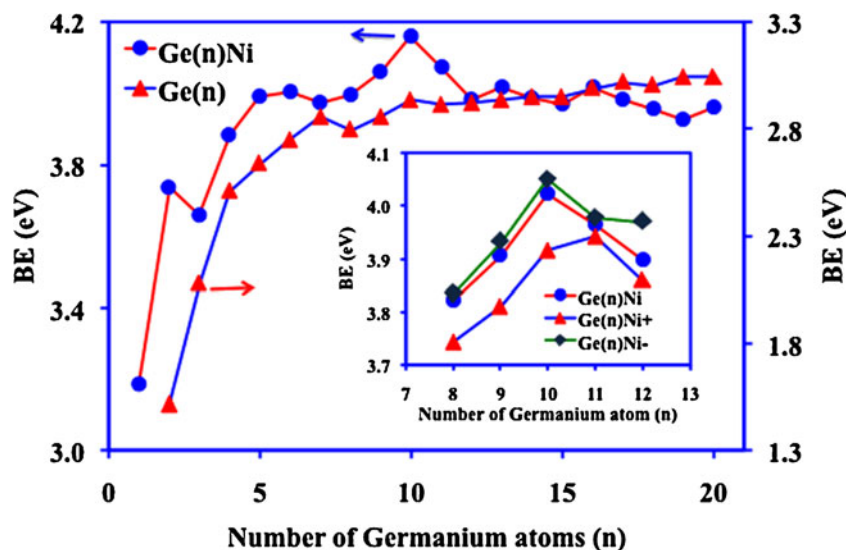


Table 2 Results of natural bond orbital (NBO) analysis of different ground state clusters

	Atom	Charge (e) ^a	Summary of natural population analysis							
			Core	Valence orbital electronic occupancies				Rydberg	Total	
Neutral Ge ₁₀ Ni cluster				4 s	4p _x	4p _y	4p _z			
	Ge	0.2595	28.00	1.557	0.906	0.774	0.774	0.016	32.027	
	Ge	0.2807	28.00	1.667	0.798	0.817	0.649	0.018	31.950	
	Ge	0.2605	28.00	1.558	0.907	0.772	0.772	0.016	32.026	
	Ge	0.2826	28.00	1.666	0.797	0.780	0.685	0.019	31.946	
	Ge	0.2832	28.00	1.665	0.797	0.646	0.820	0.018	31.947	
	Ge	0.2824	28.00	1.666	0.796	0.684	0.782	0.018	31.947	
	Ge	0.2793	28.00	1.669	0.797	0.780	0.686	0.019	31.951	
	Ge	0.2813	28.00	1.669	0.797	0.819	0.647	0.018	31.949	
	Ge	0.2788	28.00	1.670	0.798	0.650	0.816	0.019	31.953	
	Ge	0.2796	28.00	1.669	0.798	0.687	0.779	0.018	31.951	
	Ni	-2.768	17.99	Core	4 s	3d _{xy}	3d _{xz}	3d _{yz}	Rydberg	
						3d _{x₂y₂}	3d _{z₂}			
				1.852	1.896				28.351	
Cationic Ge ₁₁ Ni cluster				4 s	4p _x	4p _y	4p _z			
	Ge	0.357	28.00	1.708	0.717	0.782	0.567	0.021	31.789	
	Ge	0.347	28.00	1.666	0.875	0.713	0.567	0.017	31.838	
	Ge	0.318	28.00	1.610	0.863	0.747	0.727	0.016	31.964	
	Ge	0.383	28.00	1.703	0.641	0.639	0.794	0.020	31.797	
	Ge	0.199	28.00	1.581	0.976	0.711	0.805	0.016	32.088	
	Ge	0.368	28.00	1.633	0.753	0.738	0.686	0.019	31.830	
	Ge	0.200	28.00	1.581	0.976	0.710	0.805	0.016	32.088	
	Ge	0.369	28.00	1.634	0.753	0.740	0.685	0.019	31.830	
	Ge	0.384	28.00	1.703	0.641	0.638	0.795	0.019	31.798	
	Ge	0.194	28.00	1.507	1.034	0.776	0.775	0.015	32.107	
	Ge	0.341	28.00	1.804	0.748	0.534	0.426	0.013	31.524	
	Ni	-2.460	18.00	Core	4 s	3d _{xy}	3d _{xz}	3d _{yz}	Rydberg	
					3d _{x₂y₂}	3d _{z₂}				
				1.929	1.904				28.345	
Anionic Ge ₉ Ni cluster				4 s	4p _x	4p _y	4p _z			
	Ge	0.100	28.00	1.576	0.818	0.860	0.810	0.011	32.189	
	Ge	0.140	28.00	1.659	0.845	0.795	0.801	0.108	32.110	
	Ge	0.140	28.00	1.658	0.796	0.795	0.849	0.108	32.110	
	Ge	0.114	28.00	1.610	0.786	0.909	0.789	0.012	32.107	
	Ge	0.140	28.00	1.659	0.732	0.84	0.868	0.108	32.110	
	Ge	0.115	28.00	1.610	0.863	0.765	0.856	0.124	32.107	
	Ge	0.101	28.00	1.689	0.766	0.953	0.768	0.011	32.188	
	Ge	0.140	28.00	1.658	0.855	0.840	0.744	0.011	32.109	
	Ge	0.207	28.00	1.679	0.685	0.921	0.629	0.009	31.925	
	Ni	-2.199	17.998	Core	4 s	3d _{xy}	3d _{xz}	3d _{yz}	Rydberg	
						3d _{x₂y₂}	3d _{z₂}			
					1.906	1.922				28.042

Table 2 (continued)

	Atom	Charge (e) ^a	Summary of natural population analysis						
			Core	Valence orbital electronic occupancies				Total	
Anionic Ge ₁₀ Ni cluster				4 s	4p _x	4p _y	4p _z	Rydberg	
	Ge	0.155	28.00	1.576	1.064	0.749	0.075	0.017	31.617
	Ge	0.051	28.00	1.648	0.882	0.846	0.654	0.018	32.048
	Ge	0.153	28.00	1.577	1.064	0.748	0.748	0.017	32.154
	Ge	0.048	28.00	1.647	0.882	0.805	0.697	0.018	32.049
	Ge	0.049	28.00	1.646	0.882	0.654	0.849	0.018	32.049
	Ge	0.048	28.00	1.647	0.881	0.696	0.805	0.018	32.047
	Ge	0.051	28.00	1.650	0.880	0.804	0.698	0.018	32.05
	Ge	0.051	28.00	1.648	0.881	0.848	0.655	0.018	32.05
	Ge	0.053	28.00	1.650	0.880	0.658	0.846	0.018	32.052
Ge	0.052	28.00	1.649	0.881	0.699	0.803	0.018	32.05	
			Core	4 s	3d _{xy}	3d _{xz}	3d _{yz}	Rydberg	
Ni	0.288	17.998	0.433	1.920	1.920	1.908	0.318		
				3d _{x²-y²}	3d _{z²}				
				1.889	1.901			28.288	

^a Electronic charge $e = -1.60217646 \times 10^{-19}$ Coulomb

neutral and cationic clusters, respectively. Thus, the 20-electron rule is valid for neutral and cationic Ni@Ge_n clusters, but is not directly valid for anionic clusters. Therefore, to understand the detailed electronic charge distributions in the clusters, Mulliken natural bond orbital (NBO) analysis was performed, which allowed us to see how the valence electrons of Ge and Ni atoms are shared in bonds. In general, Ge is more electronegative than Ni; the electronegativities of Ni and Ge on the Pauling scale are 1.91 and 2.01, respectively. Mulliken population analysis also showed that, in this system, charge is always transferred from Ni to Ge, so Ni acts as an electron donor in Ge_nNi clusters. The detailed NBO analysis of the ground state icosahedral Ge₁₀Ni structure in neutral, Ge₉Ni in anionic and Ge₁₁Ni in cationic charged states is shown in Table 2. As mentioned before, according to the 20- or 18-electron counting rule, different physical and chemical parameters that can explain the thermodynamic and chemical stabilities of the clusters should show local or global peaks (maxima) or dips (minima) at $n=10$ or 8 for neutral Ni@Ge_n. However, they do show regular behavior at $n=10$ for neutral clusters, $n=10$ for anionic and $n=11$ for cationic clusters. According to the electron-counting rule, neutral Ge₁₀Ni, anionic Ge₉Ni and cationic Ge₁₁Ni are thought to be a 20-electron cluster. But the present calculated parameters of the clusters in different charged states show maxima or minima for $n=10$ (neutral and anionic) and 11 (cationic), and not for cationic Ge₉Ni. However, most of the parameters calculated for anionic clusters show neither local maxima nor a local minimum. Hence NBO analysis was performed for neutral and anionic Ge₁₀Ni and cationic Ge₁₁Ni and for anionic Ge₉Ni clusters. With reference to Table 2, in the ground state Ge₁₀Ni, Ge₁₀Ni⁻, Ge₁₁Ni⁺ and

Ge₉Ni⁻ (as shown in Fig. 1b) clusters, the valence orbital distributions of Ge atoms are limited to s, p_x, p_y, and p_z, whereas those for Ni includes, p_x, p_y, p_z, d_{xy}, d_{xz}, d_{yz}, d_{x²-y²}, d_{x²-y²} and d_{z²}. The orbital distributions of HOMO, HOMO-1, LUMO and LUMO+1 of Ge₁₀Ni, Ge₁₁Ni⁺ and Ge₉Ni⁻ are shown in Fig. 1b. From Table 2, it is clear that, among the ten valence electrons of the Ni atom in all those four clusters, all ten electrons are used to form different number of co-ordinate bonding with the Ge atoms in Ge₁₀Ni, Ge₁₁Ni⁺ and Ge₁₀Ni⁻ cages with a total of ten electrons in number. Therefore, using the free electron theory, we find that approximately 20 electrons are present in the Ge₁₀Ni, Ge₁₀Ni⁻ and Ge₁₁Ni⁺ cages. Therefore, the Ge₁₀Ni cluster in neutral, Ge₁₀Ni⁻ and Ge₁₁Ni⁺ can be considered as 20-electron clusters and show maximum binding energy. The same is true for other thermodynamic and chemical parameters of the system and will be discussed in a later section.

The EEs of the clusters were also calculated to help explain thermodynamic stability. The EE can be defined in different ways. It can be positive or negative depending on the definition used. In the present study, the embedding energy of a cluster applying the WW spin-conservation rule [67] is defined as:

$$\begin{aligned}
 EE &= -[E(^M Ge_n Ni) - E(^M Ge_n) - E(^0 Ni)] \\
 &= E(^M Ge_n) + E(^0 Ni) - E(^M Ge_n Ni)
 \end{aligned} \quad (1)$$

or

$$\begin{aligned}
 EE &= -[E(^M Ge_n Ni) - E(^0 Ge_n) - E(^M Ni)] \\
 &= E(^0 Ge_n) + E(^M Ni) - E(^M Ge_n Ni)
 \end{aligned} \quad (2)$$

where M is the total spin of the cluster or the atom in units of $h/2\pi$ and is always positive. In this case, we chose the higher of the resulting two EEs. In the present calculation, all ground states up to $n=3$ are triplet and above that all are singlet. Therefore, to calculate the EE according to the WW spin-conversion rule, pure Ge clusters were taken to be in either the triplet or the singlet state. For charged (± 1) clusters of multiplicity M , the EE of such a cluster (say cationic) can be written as:

$$\begin{aligned} EE^{WW} &= E(^2Ge_n^+) + E(^1Ni) - E(^2Ge_nNi^+) \\ &= E(^1Ge_n) + E(^2Ni^+) - E(^2Ge_nNi^+) \end{aligned} \quad (3)$$

Variation of EE with size of cluster is shown in Fig. 3. Both neutral and anionic clusters show maxima at $n=10$, whereas cationic clusters show maximum EE at $n=11$. Therefore, the neutral and cationic clusters follow the 20-electron rule directly. The sharp minima at $n=12$ for neutral and cationic cluster represent the relatively less favorable embedding nature of these clusters. Following the NBO analysis results presented in Table 2, one can get a much better idea of EE variation for neutral and charged clusters.

The stability parameter $\Delta_2(n)$ or 2nd order energy difference is defined by following the work reported by Bandyopadhyay [28] as:

$$\begin{aligned} \Delta_2(n) &= [E(Ge_{n+1}Ni) - E(Ge_nNi)] \\ &\quad - [E(Ge_nNi) - E(Ge_{n-1}Ni)] \\ &= E(Ge_{n+1}Ni) + E(Ge_{n-1}Ni) - 2E(Ge_nNi) \end{aligned} \quad (4)$$

According to this definition, greater stability means a more positive value of $\Delta_2(n)$, corresponding to a gain in energy during the growth process from the size immediately below, and less of a gain in energy to the next cluster size

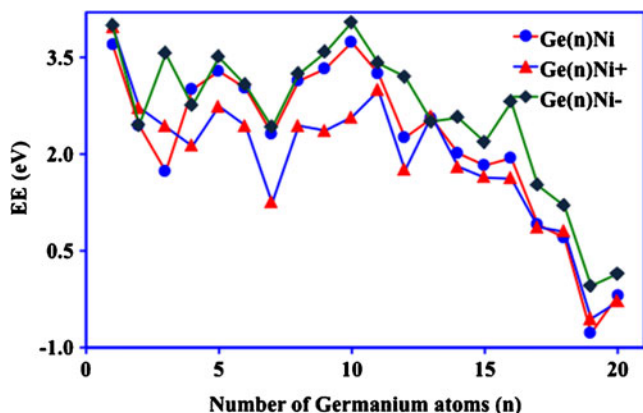


Fig. 3 Variation of embedding energy of Ge_nNi clusters in neutral and different charged states with the cluster size

up. The stabilities of neutral and charged clusters are shown in Fig. 4. The neutral cluster shows a changing nature for the series $n=8, 10, 12$ and 14 . The anionic cluster shows positive stability at $n=10$ and then shows a huge drop in stability for $n=11$ and 12 , and thus does not follow any particular series in stability nature. The cationic cluster at $n=11$ shows local maxima and this is supported by the 20-electron rule. The nature of the stability graph and the results presented in Table 2 support the relatively higher stability in 20-electron clusters: neutral $Ge_{10}Ni$, cationic $Ge_{11}Ni$ and anionic $Ge_{10}Ni$ clusters. In general, the clusters are known as “magic” clusters because of their positive and relatively higher stabilities.

Again, to investigate the growth behavior of Ge_nNi clusters, the fragmentation energy (FF) or $\Delta(n, n-1)$ was calculated starting from the Ge–Ni dimer. The FF is defined as follows:

$$\begin{aligned} \Delta(n, n-1) &= -[E(Ge_nNi) - E(Ge_{n-1}Ni) - E(Ge)] \\ &= E(Ge_{n-1}Ni) + E(Ge) - E(Ge_nNi) \end{aligned} \quad (5)$$

It is clear from Fig. 5, that there is a sharp drop in the FF from $n=10$ to 11 both in the neutral and anionic state of $Ge_{10}Ni$ cluster, whereas the FF drops sharply from $n=11$ to 12 in cationic $Ge_{11}Ni$ cluster. The sharp drop in FF for both neutral and charged clusters is an indication of maximum local stability of the $Ge_{10}Ni$ cluster. The systematic behavior of BE, EE, $\Delta_2(n)$, and $\Delta(n, n-1)$ at $n=10$ indicates that $Ge_{10}Ni$ has a relatively high thermodynamic stability. To understand the charge exchange between the cage and the embedded Ni atom during hybridization with the germanium clusters in neutral state, the variation in charge on the Ni atom and the average charge per Ge atom in the ground state $Ni@Ge_n$ clusters as a function of cluster size was calculated and is presented in Fig. 6. Like the other parameters discussed above, the charge on the Ni and Ge atoms shows a

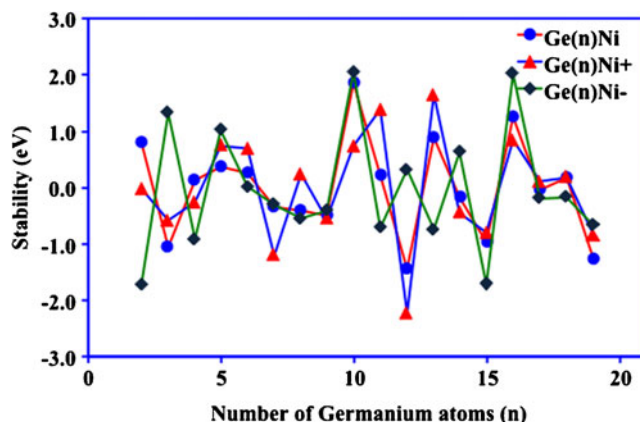


Fig. 4 Variation of stability of Ge_nNi clusters in neutral and different charged states with the cluster size

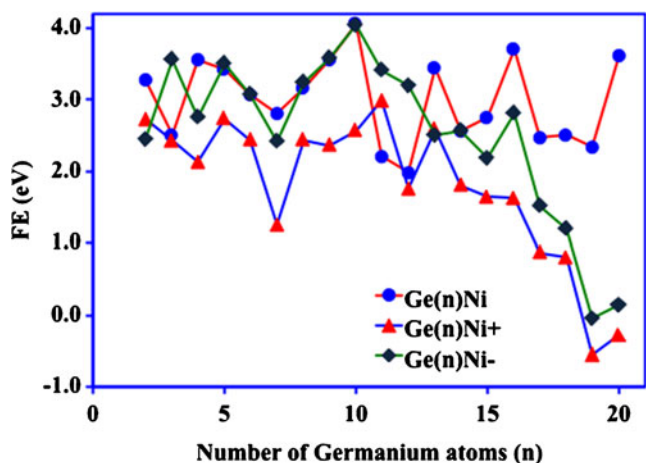


Fig. 5 Variation of fragmentation energy of Ge_nNi clusters in neutral and different charged states with the cluster size

local maximum and minimum, respectively, at $n=10$. This result provides further support for the highest relative stability of $Ge_{10}Ni$ cluster in neutral state. It is clear that the charge transferred from the Ni to Ge in the icosahedral $Ge_{10}Ni$ cage and this enhances the electrostatic interaction between the cage and the Ni atom, which plays an important role in stabilizing the $Ge_{10}Ni$ cage.

To study the kinetic stabilities of the clusters in a particular environment, the HOMO–LUMO gap (ΔE), ionization potential (IP), electron affinity (EA), chemical potential (μ), chemical hardness (η), and polarizability (α) of each cluster were calculated. In general, as ΔE increases, the reactivity of the clusters decreases. The HOMO–LUMO gaps of neutral and charged clusters are plotted in Fig. 7. As also seen for other TM-doped Si and Ge clusters [21, 22], a decreasing trend is observed for the HOMO–LUMO gap with increasing size of cluster both in neutral and charged states, with some local oscillations. In Fig. 7, there are clear local maxima

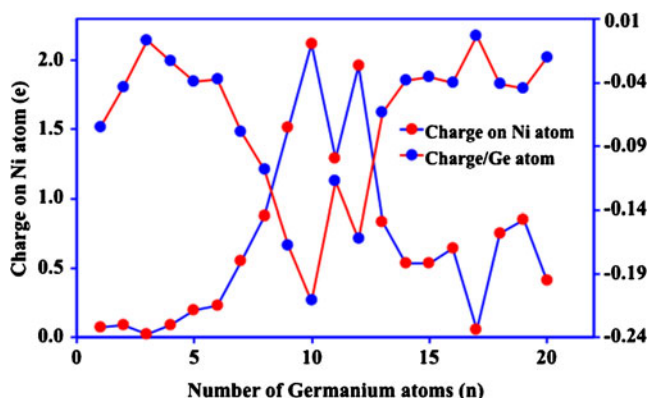


Fig. 6 Variation of charge on Ni and average charge/Ge atoms in Ge_nNi clusters with the cluster size. Here positive and negative signs represent the charge donated and received respectively

at $n=10$, 10, and 11 for neutral, anionic, and cationic Ge_nNi clusters, respectively. This again indicates that the $Ge_{10}Ni$ cluster is unusually stable, as also seen in the NBO analysis in Table 2. The main focus of the present study was to understand the relative stability of such clusters in terms of the simple electron counting rule. As reported in our previous study on metal clusters, according to the electron shell model, whenever a new shell becomes occupied for the first time, the IP drops sharply [27]. de Heer [68] has shown that, in an Li_n series, L_{20} cluster is a shell field configuration and there is a sharp drop in IP when the cluster grows from L_{20} to L_{21} . If the enhanced stability in the $Ge_{10}Ni$ cluster is due to a shell field configuration then there should be a sharp drop in IP if one more germanium atom is added to it. This can be seen clearly in Fig. 8. There is a local peak in the IP graph at $n=10$, followed by a sharp drop in IP from $n=10$ to 11. The drop in IP could be the strongest indication of the assumption of nearly free-electron gas inside the $Ge_{10}Ni$ cage cluster. The IP of a $Ge_{10}Ni$ cluster is in the same range as that of TM atoms. Hence, it may be possible to form a number of stable halides using this cluster. Discovery of such stable clusters can be helpful to identify new semiconductor TM-based “superatoms” that can be used as building blocks for future cluster-assembled designer materials.

Another parameter that can help to understand the chemical stability of a system is EA, which can be defined as:

$$EA(eV) = E(Ge_nNi) - E(Ge_nNi^-) \tag{6}$$

Under this definition, EA is always positive; clusters with greater EA are more reactive and hence are less stable. Variation in EA with cluster size is shown in Fig. 8 along with the IP of the clusters. In the graph there is a local minima at $n=10$.

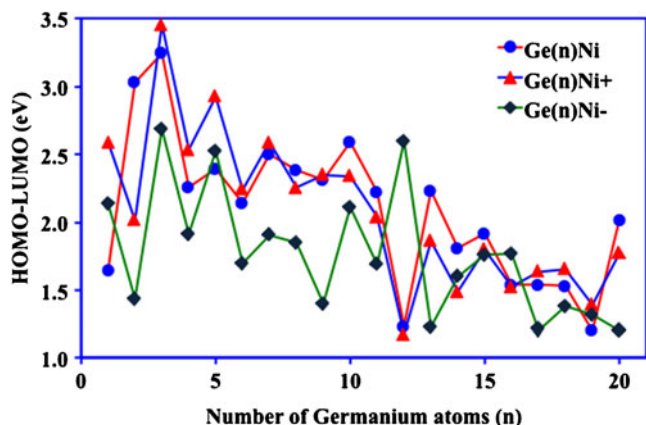


Fig. 7 Variation of HOMO-LUMO gap of Ge_nNi clusters in neutral and different charged states with the cluster size

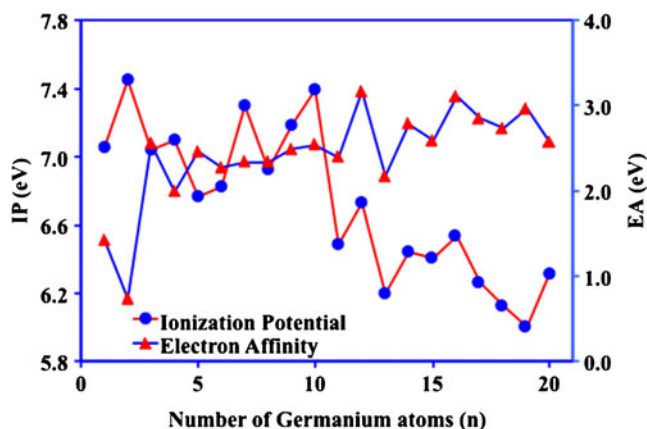


Fig. 8 Variation of ionization potential and electron affinity of Ge_nNi clusters with the cluster size

There is a hike in electron affinity from $n=10$ to 11 and it continues up to $n=12$. Then again there is a sharp drop in EA from $n=12$ to 13. A relative dip in EA at $n=10$ is an indication of enhanced stability of Ge_{10}Ni clusters in the neutral state.

Again, the maximum hardness principle (MHP) also can be used to characterize the relative stability of a system. To verify the chemical stability of Ge_nNi clusters, chemical potential (μ) and chemical hardness (η) of the ground state clusters in each size are calculated. By description of chemical potential and chemical hardness, both parameters can be expressed in terms of EA and IP. In terms of total energy considerations, if $E(n_e)$ is the energy of a ' n_e ' electron system, then energy of the system containing $n_e + \Delta n_e$ number of electrons, where $\Delta n_e \ll n_e$ can be expressed as:

$$E(n_e + \Delta n_e) = E(n_e) + \left. \frac{dE}{dn} \right|_{n=n_e} \Delta n_e + \left. \frac{1}{2} \frac{d^2E}{dn^2} \right|_{n=n_e} (\Delta n_e)^2 + \dots \text{Higher order terms} \quad (7)$$

Since a contribution from the higher order terms is negligible, μ and η can be defined as:

$$\mu = \left. \frac{dE}{dn} \right|_{n=n_e} \quad \text{and} \quad \eta = \frac{1}{2} \left. \frac{d^2E}{dn^2} \right|_{n=n_e} = \frac{1}{2} \left. \frac{d\mu}{dn} \right|_{n=n_e} \quad (8)$$

By definition, $IP = E(n_e - 1) - E(n_e)$ and $EA = E(n_e) - E(n_e + 1)$.

By setting $\Delta n_e = 1$, μ and η are related to IP and EA via the following relations:

$$\mu = -\frac{IP + EA}{2} \quad \text{and} \quad \eta = \frac{IP - EA}{2} \quad (9)$$

Consider two systems with μ_i and η_i ($i=1,2$) interacting with each other, with some amount of electronic charge

(Δq_e) transfer from one system to other. The quantity Δq_e and the resultant energy change (ΔE) due to the charge transfer can be determined in the following way:

If $E(n_e + \Delta q_e)$ is the energy of the system after charge transfer then it can be expressed for two different systems 1 and 2 in the following way:

$$E_1(n_{1e} + \Delta q_e) = E_1(n_{1e}) + \mu_1(\Delta q_e) + \eta_1(\Delta q_e)^2 \quad \text{and} \\ E_2(n_{2e} - \Delta q_e) = E_2(n_{2e}) - \mu_2(\Delta q_e) + \eta_2(\Delta q_e)^2 \quad (10)$$

Corresponding chemical potentials become,

$$\mu'_1 = \left. \frac{dE_1(n + \Delta q_e)}{dn} \right|_{n=n_{1e}} = \mu_1 + 2\eta_1 \Delta q_e \quad \text{and} \\ \mu'_2 = \left. \frac{dE_2(n - \Delta q_e)}{dn} \right|_{n=n_{2e}} = \mu_2 - 2\eta_2 \Delta q_e \quad (11)$$

When the systems are in chemical equilibrium, i.e. $\mu'_1 = \mu'_2$, one can obtain the charge transfer and energy gain by the following expressions:

$$\Delta q_e = \frac{\mu_2 - \mu_1}{2(\eta_1 + \eta_2)} \quad \text{and} \quad \Delta E = \frac{(\mu_2 - \mu_1)^2}{2(\eta_1 + \eta_2)} \quad (12)$$

In the above expressions, ΔE is the gain in energy by the total system (1 and 2) due to exclusive alignment of chemical potential of the two systems at the same value. Thus, for easier charge transfer from one system to other it is necessary to have a large difference in μ together with low η_1 and η_2 . Therefore, Δq_e and ΔE can be taken as the factors to gain an idea about the reaction affinity between two systems. Since they are functions of the chemical potential and chemical hardness of the systems, it is important to calculate these parameters to determine the chemical stability in a particular environment.

Using the above theoretical background, chemical potential (μ) and chemical hardness (η) of $\text{Ni}@\text{Ge}_n$ clusters were calculated and are presented in Fig. 9. The local minima of μ at $n=10$ is an indication of higher stability compare to the surrounding sizes. Variation in η , which is a measure of chemical affinity (considering covalent type of bonding), show local maxima at $n=10$. This local maximum is the measure of hardness of electronic clouds surroundings the cluster to oppose any kind of shearing in chemical bonding with external agencies. Therefore, the peak at $n=10$ indicates the higher stability. Again to understand the effect of η on polarizability, the polarizability parameter was calculated and is plotted in Fig. 10. Following earlier theoretical work [69, 70], in covalent-type bonding more hardness usually indicates lower polarizability. This is clear from Figs. 9 and 10. To some extent, the electrostatic dipole moment of the cluster is also related to the atomic polarizability and the

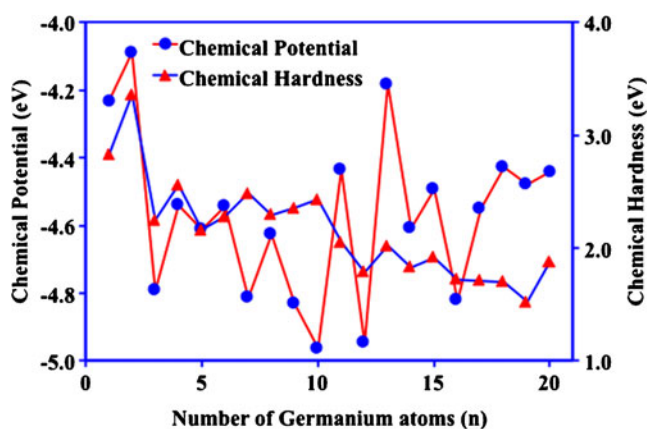


Fig. 9 Variation of chemical potential and chemical hardness of Ge_nNi clusters with the cluster size

cluster structure. In a symmetrical cage-like structure where the Ni atom is at the center of the cage, the electrostatic dipole moment of the cluster is usually very low, as in, for example, ground state 10A clusters. The dipole moments in the clusters increase suddenly when a germanium atom is dropped or added to the clusters. The ground state clusters within the size range between $n=9$ to 16 are all cage types with endohedrally doped Ni. The dipole moments of these clusters varies from 0 to 0.47 Debye. In the whole range of this study, the first dipole moment of the clusters decreases to zero, or a very low value, within the range from $n=10$ to 15 and then again tends to increase when distortion in the cage begins.

Conclusions

The present theoretical study reports the growth behavior, stability, electronic and different chemical and physical properties of $\text{Ni}@\text{Ge}_n$ clusters within the size range of $n=1$ to 20 under spin polarized generalized gradient approximation

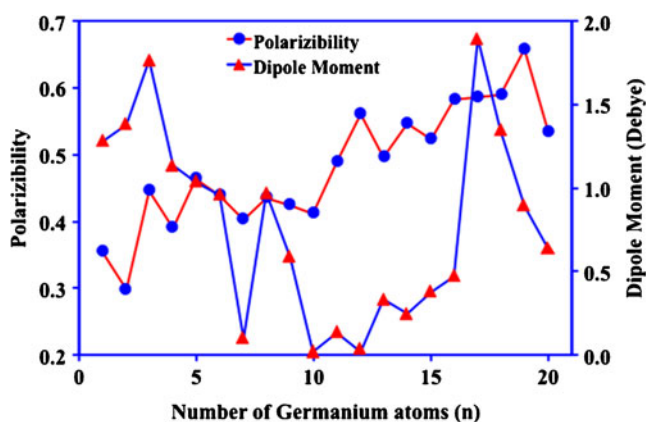


Fig. 10 Variation of polarizability and electrostatic dipole moment of Ge_nNi clusters with the cluster size

(GGA) using B3LYP method. Different physical and chemical properties of the optimized clusters are discussed. Based on the results, the following conclusions have been drawn:

1. The growth pattern of Ge_nNi clusters can be grouped mainly into two categories. In the smaller size range, i.e., before encapsulation of the Ni atom, Ni or Ge atoms are added directly with the Ge_n or Ge_{n-1}Ni to form Ge_nNi clusters, where the binding energy of small clusters increases at a much faster rate than bigger sized clusters. After encapsulation of the Ni atom by the Ge_n cluster with $n>7$, the size of the Ge_nNi cluster tends to increase by absorbing Ge atoms one by one onto its surface, keeping the Ni atom inside the cage.
2. Addition of the Ni-atom to Ge clusters was always found to be favorable at all sizes, as the EE turns out to be positive (following the present definition) in every case of neutral and charged clusters. All ground state clusters with size $n>7$ absorb Ni endohedrally in the cage of Ge_n pure cluster.
3. From the calculated results of BE, EE, $\Delta(n,n-1)$ and $\Delta_2(n)$, the clusters Ge_{10}Ni , $\text{Ge}_{10}\text{Ni}^-$ and $\text{Ge}_{11}\text{Ni}^+$ were found to be most stable. Detailed NBO analysis showed that the neutral and charged clusters with nearly 20 valence electrons in total show enhanced stability, in agreement with shell model predictions. This also shows up in the IP values of the Ge_nNi clusters, as there is a sharp drop in IP from $n=10$ to 11. Although the signature of stability is not as sharp in the HOMO-LUMO gap of the charged clusters, there is a local maximum at $n=10$ in the neutral state. This is an indication of enhanced stability in the 20-electron cluster. Other parameters, like EA and chemical potential, are related to the chemical stabilities and hardness along with polarizability, and the dipole moment of the neutral cluster for $n=10$ also supports the identical nature of cluster stability.
4. As mentioned above, the drop in adiabatic IP in the present calculations during the growth process is one of the strongest lines of evidence for the presence of nearly free-electron gas inside the Ge_{10}Ni cage cluster. In this context, it is important to mention that the B3LYP functional is not very effective for extended quasi-metallic systems [71]. However, its effectiveness in the present calculation could be due to the nano-order clusters of the system. Since the IP of a Ge_{10}Ni cluster is in the same range as that of TM atoms, it may be possible to form a number of stable halides using this cluster, and it may be possible to invent new semiconductor-TM metal-based “superatoms” that can be the building blocks for future cluster-assembled designer materials and thus open up new fields in the electronics industry. The present work represents a first step in this direction.

Acknowledgment Complete computations using Gaussian'03 were performed at the cluster computing facility, Harish-Chandra Research Institute, Allahabad, UP, India (<http://cluster.hri.res.in>).

References

1. Ho KM, Shvartsberg AA, Pan B, Lu ZY, Wang CZ, Wacker JG, Fye JL, Jarrod MF (1998) *Nature* 392:582
2. Lokibe K, Tachikawa H, Azumi K (2007) *J Phys B Atomic Mol Opt Phys* 40:427
3. Shvartsberg AA, Jarrod MF (1999) *Phys Rev A* 60:1235
4. Jarrod MF, Constant VA (1991) *Phys Rev Lett* 67:2994
5. Benedict LX, Puzer A, Willimson AJ, Grossman JC, Galli G, Klepeis JE, Raty JY, Pankratov O (2003) *Phys Rev B* 68:85310
6. Brown WL, Freeman RR, Raghavachari K, Schluter M (1987) *Science* 235:860
7. Hiura H, Miyazaki T, Kanayama T (2001) *Phys Rev Lett* 86:1733
8. Hayashi S, Kanzaya Y, Kataoka M, Nagarede T, Yamamoto K (1993) *Z Phys D Atom Mol Clusters* 26:144
9. Rothlisberger U, Andreoni W, Parrinello M (1994) *Phys Rev Lett* 72:665
10. Kaxiras E, Jackson K (1993) *Phys Rev Lett* 71:727
11. Gopakumar G, Lievens P, Nguyen MT (2006) *J Chem Phys* 124:214312
12. Li S, Van Zee RJ, Weltner W Jr, Raghavachari K (1995) *Chem Phys Lett* 243:275
13. Rata I, Shvartsberg AA, Horoi M, Frauenheim T, Michael Siu KM, Jackson KA (2000) *Phys Rev Lett* 85:546
14. Jarrod MF, Bower JE (1992) *J Chem Phys* 96:9180
15. Kumar V, Kawazoe Y (2001) *Phys Rev Lett* 87:045503
16. Kumar V, Kawazoe Y (2002) *Phys Rev Lett* 88:235504
17. Beck SM (1987) *J Chem Phys* 87:4233
18. Beck SM (1989) *J Chem Phys* 90:6306
19. Ohara M, Miyajima K, Pramann A, Nakajima A, Kaya K (2002) *J Phys Chem A* 106:3702
20. Bandyopadhyay D, Sen P (2010) *J Phys Chem A* 114:1835
21. Bandyopadhyay D (2008) *J Appl Phys* 104:084308
22. Bandyopadhyay D (2009) *Mol Simul* 35:381
23. Bandyopadhyay D (2012) *J Mol Model* 18:737
24. Bandyopadhyay D (2009) *Eur Phys J D* 54:643
25. Bandyopadhyay D, Kumar M (2008) *Chem Phys* 353:170
26. Kumar M, Bhattacharyya N, Bandyopadhyay D (2012) *J Mol Model* 18:405
27. Bandyopadhyay D, Kaur P, Sen P (2010) *J Phys Chem A* 114:12986
28. Bandyopadhyay D (2012) *J Mol Model* 18:3887
29. Koyasu K, Akutsu M, Mitsui M, Nakajima A (2005) *J Am Chem Soc* 127:4998
30. Kawamura H, Kumar V, Kawazoe Y (2005) *Phys Rev B* 71:075423
31. Yang JC, Lin L, Zhang Y, Jalbout AF (2008) *Theor Chem Account* 121:83
32. Marchal R, Carbonniere P, Pouchan C (2010) *Int J Quantum Chem* 110:2256
33. Karamanis P, Marchal R, Carbonniere P, Pouchan C (2011) *J Chem Phys* 135:044511
34. Zhang X, Li G, Gao Z (2001) *Rapid Commun Mass Spectrom* 15:1573
35. Wang J, Han JG (2006) *J Chem Phys B* 110:7820
36. Han JG, Ren YZ, Zhang YW (2004) *Chem Phys* 305:253
37. Deutsch PW, Curtiss LA, Blaudeau JP (1997) *Chem Phys Lett* 270:413
38. Li BX, Cao PL (2000) *Phys Rev B* 62:15788
39. Wang JL, Yang M, Wang GH, Zhao JJ (2003) *Chem Phys Lett* 367:448
40. Bandyopadhyay D (2009) *Nanotechnology* 20:275202
41. Reveles JU, Clayborne PA, Reber AC, Khanna SK, Pradhan K, Sen P, Pederson MP (2009) *Nat Chem* 1:310
42. Aguado A (2012) *J Phys Chem C* 116(12):6841
43. Lee C, Yang W, Parr RG (1988) *Phys Rev B* 37:785
44. Frisch MJ, Trucks GW, Schlegel HB, Scuseria GE, Robb MA, Cheeseman JR, Zakrzewski VG, Montgomery Jr JA, Stratmann RE, Burant JC, Dapprich S, Millam JM, Daniels AD, Kudin KN, Strain MC, Farkas O, Tomasi J, Barone V, Cossi M, Cammi R, Mennucci B, Pomelli C, Adamo C, Clifford S, Ochterski J, Petersson GA, Ayala PY, Cui Q, Morokuma K, Malick DK, Rabuck AD, Raghavachari K, Foresman JB, Cioslowski J, Ortiz JV, Baboul AG, Stefanov BB, Liu B, Liashenko A, Piskorz P, Komaromi I, Gomperts R, Martin RL, Fox DJ, Keith T, Al-Laham MA, Peng CY, Nanayakkara A, Challacombe M, Gill PMW, Johnson B, Chen W, Wong MW, Andres JL, Gonzalez C, Head-Gordon M, Replogle ES, Pople JA (2004) *Gaussian 03, revision E01* Gaussian, Wallingford
45. Hay PJ, Wadt WR (1985) *J Chem Phys* 82:270
46. Hay PJ, Wadt WR (1985) *J Chem Phys* 82:284
47. Hay PJ, Wadt WR (1985) *J Chem Phys* 82:299
48. Islam MS, Ray AK (1988) *Chem Phys Lett* 153:496
49. Northrup E, Cohen ML (1983) *Chem Phys Lett* 102:440
50. Pacchioni G (1984) *Chem Phys Lett* 107:70
51. Pacchioni G, Koutecky J (1986) *J Chem Phys* 84:3301
52. Dai D, Balasubramanian K (1992) *J Chem Phys* 96:8345
53. Deutsch PW, Curtiss LA, Blaudeau JP (1997) *Chem Phys Lett* 270:413
54. Abtey TA, Drabold DA (2007) *Phys Rev B* 75:045201
55. Nagendran S, Sen SS, Roesky HW, Koley D, Grubmüller H, Pal A, Herbst-Irmer R (2008) *Organometallics* 27:5459
56. Bell NA, Glockling F, Schneider ML, Shearer HMM, Wilbey MD (1984) *Acta Crystallogr C* 40:625
57. Shim I, Kingcade JE, Gingerich KA (1988) *J Chem Phys* 89:3104
58. Reddy BV, Nayak SK, Khanna SN, Rao BK, Jena P (1998) *J Phys Chem A* 102:1748
59. Ho J, Polak ML, Ervin KM, Lineberger WC (1993) *J Chem Phys* 99:8542
60. Grigoryan VG, Springborg M (2001) *Phys Chem Chem Phys* 3:5135
61. Noell JO, Newton MD, Hay PJ, Martin RL, Bobrowicz FW (1980) *J Chem Phys* 73:2360
62. Kohn W, Sham LJ (1965) *Phys Rev* 140:A1133
63. Tai TB, Nguyen MT (2011) *J Chem Theory Comput* 7:1119
64. Calvo F (2009) *Comput Mater Sci* 40:8
65. Marchal R, Carbonniere P, Pouchan C (2009) *J Chem Phys* 131:114105
66. Avaltroni F, Corminboeuf CC (2012) *J Comput Chem* 33:502
67. Wigner E, Witmer EE (1928) *Z Phys* 51:859
68. de Heer WA (1993) *Rev Mod Phys* 65:611
69. Hati S, Datta D (1994) *J Phys Chem* 98:10451
70. Ghanti TK, Ghosh SK (1994) *J Phys Chem* 98:9197
71. Paier J, Marsman M, Kresse G (2007) *J Chem Phys* 127:024103